Journal of Nuclear Materials 480 (2016) 271–280

Contents lists available at ScienceDirect

Journal of Nuclear Materials

journal homepage: www.elsevier.com/locate/jnucmat

Phase decomposition of γ-U (bcc) in U-10 wt% Mo fuel alloy during hot isostatic pressing of monolithic fuel plate

Y. Park [a], N. Eriksson [a], R. Newell [a], D.D. Keiser [b], Y.H. Sohn [a, *]

[a] Department of Materials Science and Engineering, Advanced Materials Processing and Analysis Center, University of Central Florida, Orlando, FL 32816, USA

[b] Idaho National Laboratory, PO Box 1625, Idaho Falls, ID 83401, USA

ARTICLE INFO

Article history:
Received 2 June 2016
Received in revised form
17 August 2016
Accepted 18 August 2016
Available online 20 August 2016

ABSTRACT

Eutectoid decomposition of γ-phase (cI2) into α-phase (oC4) and γ′-phase (tI6) during the hot isostatic pressing (HIP) of the U-10 wt% Mo (U10Mo) alloy was investigated using monolithic fuel plate samples consisting of U10Mo fuel alloy, Zr diffusion barrier and AA6061 cladding. The decomposition of the γ-phase was observed because the HIP process is carried out near the eutectoid temperature, 555 °C. Initially, a cellular structure, consisting of γ′-phase surrounded by α-phase, developed from the destabilization of the γ-phase. The cellular structure further developed into an alternating lamellar structure of α- and γ′-phases. Using scanning electron microscopy and transmission electron microscopy, qualitative and quantitative microstructural analyses were carried out to identify the phase constituents, and elucidate the microstructural development based on time-temperature-transformation diagram of the U10Mo alloy. The destabilization of γ -phase into α- and γ′-phases would be minimized when HIP process was carried out with rapid ramping/cooling rate and dwell temperature higher than 560 °C.

1. Introduction

The replacement of high-enriched uranium (HEU) fuel with low-enriched uranium (LEU) fuel is the primary goal of Materials Management and Minimization Reactor Conversion (MMMRC) program, also known as Reduced Enrichment for Research and Test Reactor (RERTR) program [1–4]. Uranium based metallic fuel has garnered heavy consideration based on several advantageous properties, including high fissionable density, high thermal conductivity and good compatibility with cladding materials.

Monolithic design using U-10 wt%Mo (U10Mo) fuel alloy is being developed to achieve a higher uranium density for high flux reactors, because of high fissionable density and excellent irradiation behavior [5–7]. The monolithic fuel plates are fabricated via hot isostatic pressing (HIP) in order to encase the fuel plate foil in an Al-alloy based cladding. A Zr diffusion barrier is typically placed between the U10Mo fuel alloy and Al-alloy cladding to prevent interaction between the fuel and cladding. Previously, microstructure resulting from the interdiffusion and solid-state reaction between different constituents of the fuel plate was reported [8–13]. In addition, within the fuel alloy, Meyer *et* al. [11] reported the presence of "chemical banding" with inhomogeneous Mo content within the fuel alloy, and Jue *et* al. [12] identified γ-phase decomposed regions consisting of α and γ′ phases due to heat treatment near the eutectoid temperature. The low-Mo (~5 wt %) and high-Mo (~13 wt%) phases were assumed as α and γ′, respectively [12]. In this study, decomposition of γ-U10Mo (γ) into α-U (α) and γ′-U_2Mo (γ′) was examined in detail by electron diffraction and quantitative image analysis, because the HIP process is carried out near the eutectoid temperature [14].

2. Background

Pure U exhibits two allotropic transformations, and thus three different crystal structures. Orthorhombic α-, tetragonal β- and body-centered cubic (BCC) γ-phases are stable up to 667 °C, between 667° and 771 °C, and above 771 °C, respectively [14–17]. The α-U has undesirable characteristics as a nuclear fuel such as low hardness, rapid oxidation, low corrosion resistance and anisotropic irradiation behavior [18–21]. A single crystal of α shortens in a-axis and extends in b-axis, and there is no significant change in c-axis

* Corresponding author. Department of Materials Science and Engineering and Advanced Materials Processing and Analysis Center, University of Central Florida, Orlando, FL 32816, USA.
E-mail address: yongho.sohn@ucf.edu (Y.H. Sohn).

http://dx.doi.org/10.1016/j.jnucmat.2016.08.022
0022-3115/

during irradiation under 500 °C [16,22], leading to dimensional instability [23,24].

In contrast, the γ-phase exhibits favorable properties as a nuclear fuel. The bcc γ displays good dimensional stability because of isotropic expansion during irradiation [24]. The γ-phase also has a higher corrosion resistance to water, both liquid and vapor [25]. In order to retain the metastable γ-phase below 560 °C, rapid cooling or alloying additions has been employed [26,27]. It is difficult for pure U to exist as γ-phase even after quenching, because α-phase is thermodynamically favorable at low temperature [24,26,27]. Thus, alloying U with Mo or Zr or Nb has been adopted to stabilized the γ-phase and produce good irradiation behavior [28–30]. Table 1 shows the characteristics of potential alloying elements in U. Mo, Zr and Nb have been considered because of appropriate characteristics such as low neutron absorption, high melting point, high thermal conductivity and good corrosion resistance among all elements. U-Mo has been selected for higher uranium density, stabilization of γ-phase, favorable properties listed in Table 1, despite the higher thermal neutron absorption and thermal conductivity, and excellent irradiation behavior [5,6,24,29,31].

The γ decomposition is affected by the Mo concentration in the alloy. The time-temperature-transformation (T-T-T) diagram presented in Fig. 1 [27] demonstrates that the decomposition is hindered by the Mo addition. With the Mo content 8 wt% or above, the γ-phase is stabilized even from slow cooling with acceptable uranium density for good irradiation behavior [32].

Despite the sluggish kinetics, according to the equilibrium phase diagram, the high-temperature γ-phase undergoes a eutectoid decomposition upon cooling into low-temperature orthorhombic α- and tetragonal γ'-phases as shown in Fig. 2 [14,33–36]. The equilibrium temperature of decomposition is relevant to the high temperature employed during co-rolling and HIP for the monolithic fuel system. Table 2 lists selected and relevant properties of the γ-, α- and γ'-phases. Generally, the microstructure related to the decomposition was observed first at γ-phase grain boundaries [28,37].

Fig. 3 presents the T-T-T diagram that illustrates the time-dependent phase decomposition of the γ-phase in U10Mo alloy. The T-T-T diagrams of Repas *et* al. [26] and Peterson *et* al. [27] were constructed based on hardness, dilatometry, XRD and metallographic analyses. Saller *et* al. [37] also reported measurements of the electrical resistivity and hardness for U-21 at.% Mo alloy, indicating a structural transformation from BCC to an ordered body-centered tetragonal through isothermal transformation study at 500 °C. The transformation began approximately at 27 h and completed around 170 h. It should be noted that a reverse decomposition, i.e., α and γ′ into γ was observed during irradiation testing [38,39].

Fig. 4 shows a typical backscatter electron (BSE) micrograph of the HIP fuel plate investigated in this study. The U10Mo fuel alloy was cladded in AA6061 with a Zr diffusion barrier in-between. Microstructure of the U10Mo alloy in HIP fuel plates was characterized by scanning electron microscopy (SEM), transmission electron microscopy (TEM), and a variety of analytical techniques including X-ray energy dispersive spectroscopy (XEDS). Quantitative image analyses were carried out to estimate volume fraction of decomposed regions based on BSE micrographs.

Table 1
Elemental characteristics of Mo, Zr and Nb [42–44].

Property	Mo	Zr	Nb
Thermal neutron absorption (barn)	2.48	0.18	1.15
Density (gcm^{-3})	10.22	6.49	8.35
Melting point (°C)	2623	1854	2477
Thermal expansion coefficient (K^{-1})	5.35×10^{-6}	5.78×10^{-6}	7.34×10^{-6}
Thermal Conductivity ($Wm^{-1}K^{-1}$)	138	22.7	54
Corrosion resistance	Good	Good	Good

3. Experimental details

The U10Mo alloy was fabricated by arc-melting pellets of depleted U and 99.95% pure Mo which were cleaned with 30% nitric-acid to remove oxidation at the surface. The melting process was carried out in a vacuum of 1.3×10^{-3} Pa (10^{-5} Torr) containing less than 50 ppm oxygen, and the U10Mo alloy was turned and re-melted three times in graphite crucible to ensure the homogeneity. The cast U10Mo alloy had an approximate dimension of $88.8 \times 48.9 \times 3.2$ mm and a carbon content of approximately 700 ppm. The ingot was laminated in a carbon steel can using a pure Zr (99.9% pure) foil with a starting thickness of 250 μm on each surface. A ~30% nitric acid solution was used to etch the reactor-grade Zr prior to lamination. The Zr-laminated U10Mo coupon, pre-heated at 650 °C for 30 min in a furnace, was co-rolled 15 times to a thickness of approximately 0.46 mm. Subsequently, a post-rolling heat treatment was performed at 650 °C for 45 min. The hot-rolled and annealed foil was removed from the can, and cold-rolled to a final thickness of 0.33 mm. The final dimension of as-rolled foil was approximately $746 \times 65 \times 0.33$ mm. The foil was exposed for approximately 130 min at 650 °C. The final thickness of the Zr diffusion barriers on each surface was approximated at 25 μm. Each small U-Mo foil sectioned from the as-rolled parent foil was used in this study. In general, each small foil sample exhibited the same microstructure in the co-rolled U10Mo/Zr laminate previously observed by Park *et* al. [9]. "AR" in this study is defined as the as-co-rolled/sectioned sample prior to the HIP process.

The polished AR sample (each U10Mo/Zr mini foil) was cleaned using a mixture of nitric and hydrofluoric acid (2.5% HF, 35% HNO_3 and 62.5% H_2O), and any residual oxide scale of AA6061 cladding was removed by etching using a 1.85 M NaOH and then a 30% nitric acid solution. After cleaning, the AR samples were rinsed with ethanol and stacked with AA6061 (in wt.% nominal composition of 0.6Si–0.35Fe–0.28Cu–0.08Mn–1.0Mg–0.20Cr–0.13Zn–0.08Ti–Al balance) cladding pieces. The U10Mo/Zr minifoil was then HIP'ed with the AA6061 at various temperatures (520, 540, 560 and 580 °C) and durations (45, 60, 90 180 and 345 min). The U10Mo/Zr/AA6061 assemblies were placed into stainless steel HIP cans with tool-steel strong-backs that were welded with corners open for degassing in an argon atmosphere glove box. The assemblies were subsequently leak-checked and vacuum degassed at 315 °C for 3 h. After loading into a laboratory-size HIP, the HIP cans were heated with heat-up and cool-down rates (H/C rate) of 35, 70 and 280 °C/h to the target temperature. The isostatic pressure of 103 MPa (15 ksi) for HIP process was applied in an argon environment. The samples characterized as functions of HIP parameters in this study are listed in Table 3.

After fabrication, the fuel plates were cross-sectioned and mounted in epoxy. The mounted fuel plates were polished using silicon carbide papers (240, 600, 800 and 1200 grits) with an ethanol lubricant. Final polishing was carried out utilizing diamond pastes (3 and 1 μm) with an oil lubricant in an Ar glove box to prevent oxidation and contamination. Microstructural features in U10Mo solid solution were examined utilizing a Zeiss ULTRA-55 field-emission SEM with XEDS capabilities. High-contrast in back-scatter electron micrographs were utilized to distinguish the different phases and quantitative analyses. Transmission electron microscopy (FEI/Tecnai™ F30) equipped with Fischione™ high angle annular dark-field (HAADF) and XEDS were used to examine the detailed microstructures and identify the phase constituents via selected area electron diffraction (SAED) and high resolution

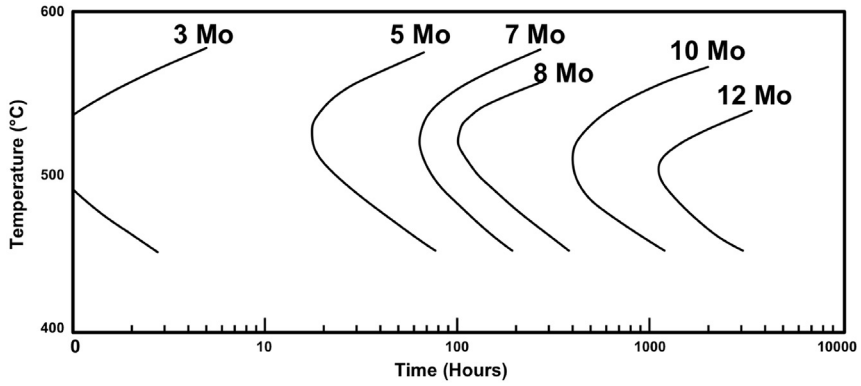

Fig. 1. Time-temperature-transformation diagram of U-Mo alloys as a function of Mo content [26].

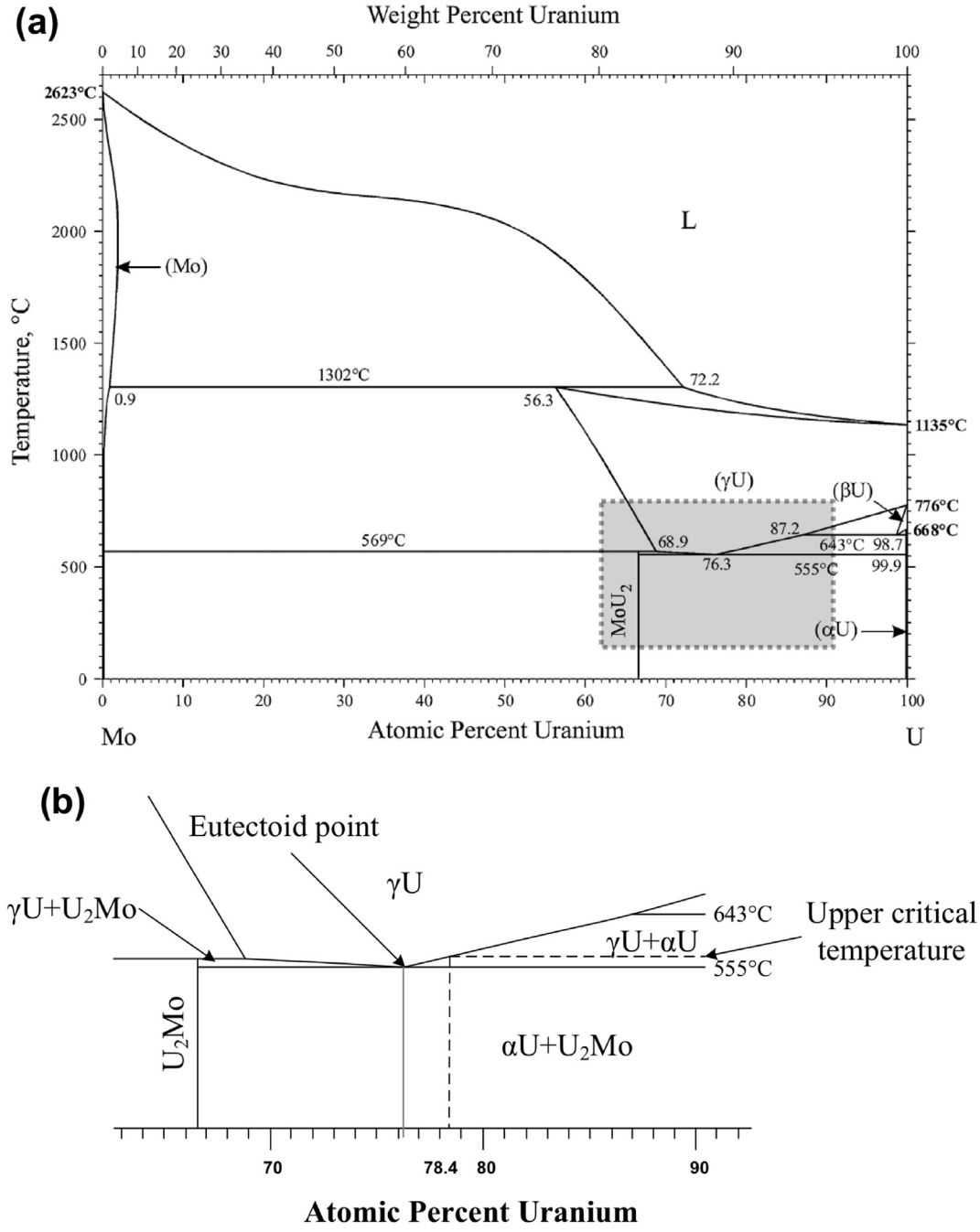

Fig. 2. (a) Equilibrium phase diagram for the U-Mo system with (b) a magnified view of the γ Û α+γ′ eutectoid reaction [14].

Table 2
Selected properties of γ-U (U − 10 wt% Mo), α-U and γ′-U_2Mo phases [14,23,32,40,41,45–51,52].

Property		γ-(U10Mo) (at 800 °C)	α-U (at 627 °C)	γ′-(U_2Mo) (at 500 °C)
Mo solubility (wt.%)		10	0.2	16
Strukturbericht designation		A2	A20	C11b
Prototype		W	α-U	$MoSi_2$
Crystal structure		Body-centered cubic	C-centered orthorhombic	Body-centered tetragonal
Lattice parameter (Å)	a	3.474	2.854	3.427
	b	3.474	5.869	3.427
	c	3.474	4.955	9.834
Space group		Im3m (229)	Cmcm (63)	I4/mmm (139)
Pearson symbol		cI2	oC4	tI6
Young's modulus (GPa)		98	117	102
Hardness (GPa)		3.1	2.3	N/R
Poisson ratio		0.35	0.26	0.40
Thermal conductivity ($W \cdot m^{-1}K^{-1}$)		3.65	34	N/R
Thermal expansion coefficient (10^{-6} K^{-1})		19.2	18.0	14.7
Specific heat ($J \cdot K^{-1}g^{-1}$)		0.194	0.192	0.154

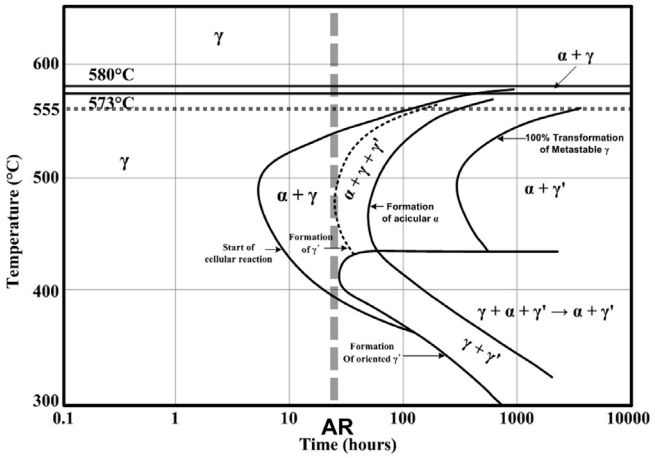

Fig. 3. Time-temperature-transformation diagram of the U - 10 wt.% Mo alloy [24]. "AR" represents the time-coordinate of the alloy in as-co-rolled condition, based on microstructural analysis.

TEM (HRTEM). The TEM samples were prepared by focused ion beam and an in-situ lift-out process was utilized for sample extraction (FIB-INLO; FEI™ TEM200) using site-specific capability. Typical phase constituents and microstructural developments due to interdiffusion and reaction at the U10Mo/Zr and Zr/AA6061 interfaces in these samples were reported previously [8,9]. This paper reports, in detail, the phase transformation of γ-phase in the U10Mo fuel alloy as functions of HIP temperature, holding time and ramping/cooling (H/C) rate as listed in Table 3.

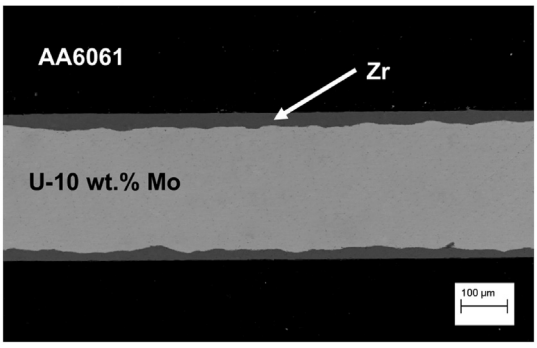

Fig. 4. Typical backscatter electron micrograph of the U10Mo monolithic fuel encased in AA6061 with Zr diffusion barrier, produced by co-rolling and hot-isostatic pressing (sample 56-345, hot-isostatic pressed at 560 °C for 345 min) [9].

Table 3
Hot isostatic pressing parameters of monolithic fuel plate specimens examined in this study.

Sample identification	Temp. (°C)	Hold time (min)	Ramp rate (°C/hr)
AR	N/A	N/A	N/A
52-90-280	520	90	280
54-90-280	540	90	280
56-90-280	560	90	280
58-90-280	580	90	280
56-45-280	560	45	280
56-60-280	560	60	280
56-180-280	560	180	280
56-345-280	560	345	280
56-90-35	560	90	35
56-90-70	560	90	70

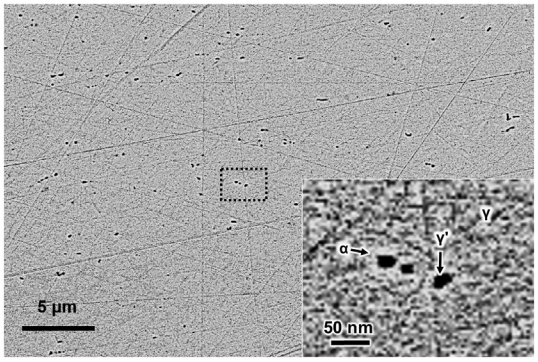

Fig. 5. Backscatter electron micrograph of the cellular structure observed from the decomposition of γ into α and γ′ found in the as-co-rolled U - 10 wt.% Mo alloy prior to hot-isostatic pressing.

4. Result and discussion

The AR sample before HIP process exhibited a small amount of cellular structure which consists of α-, γ- and γ'-phases as shown in Fig. 5. The cellular structure is assumed as the initial feature associated with onset of γ'-formation (i.e., start of the α+ γ+ γ′ phase region in Fig. 3) prior to development of lamellar structure, and is also assumed to nucleate at heterogeneous sites, such as grain boundaries. Only the cellular structure without any lamellar

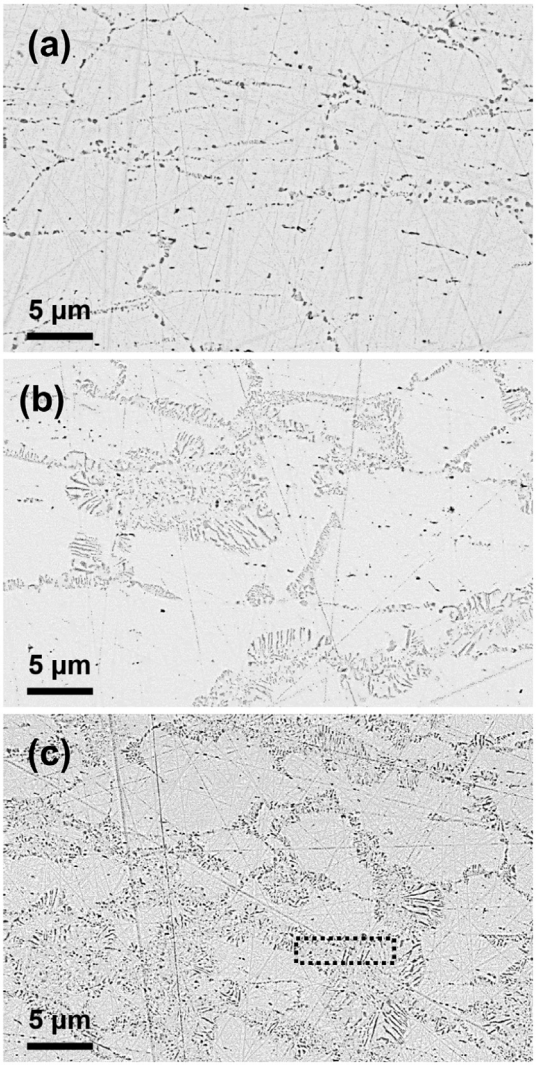

Fig. 6. Backscattered electron micrographs from the U - 10 wt.% Mo alloy in the monolithic fuel plates HIP'ed at 560 °C for 90 min with variation in heating/cooling rate: (a) 280, (b) 70, and (c) 35 °C/hour.

features were observed in the AR sample. The cellular structure is also characterized by the Mo depleted regions surrounding the Mo-rich γ′ nuclei as shown by the inset in Fig. 5. Based on these observations, AR sample is assumed to exhibit features characteristic of an U10Mo alloy corresponding to a time coordinate of 25 h in the U10Mo T-T-T diagram as labeled in Fig. 3. In other words, subsequent HIP and the corresponding characterization results assume that the starting coordinates for U10Mo alloy fuel in T-T-T diagram is at 25 h as labeled in Fig. 3.

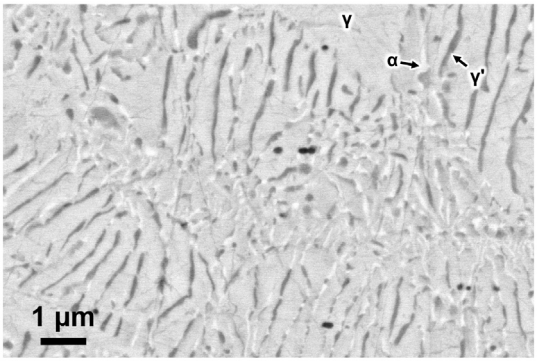

Fig. 7. High magnification backscatter electron micrograph from the lamellar structure consisting of alternating α and γ′ phases observed in the U - 10 wt.% Mo alloy, HIP'ed into monolithic fuel plates at 560 °C for 90 min with heating and cooling rate of 35 °C/hour, shown in Fig. 6(c).

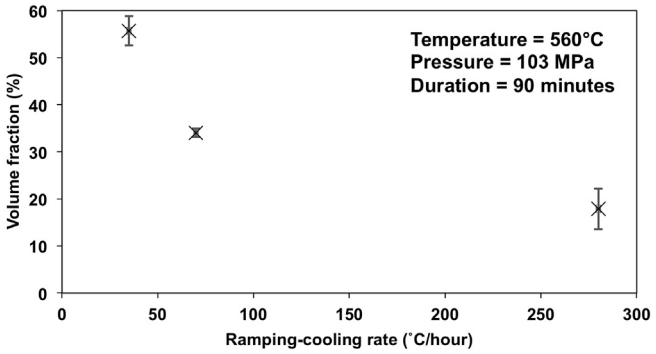

Fig. 8. Volume fraction estimated for the decomposed (i.e., cellular and lamellar structures) region in the U - 10 wt.% Mo alloy, HIP'ed into monolithic fuel plates at 560 °C for 90 min as a function of heating/cooling rate.

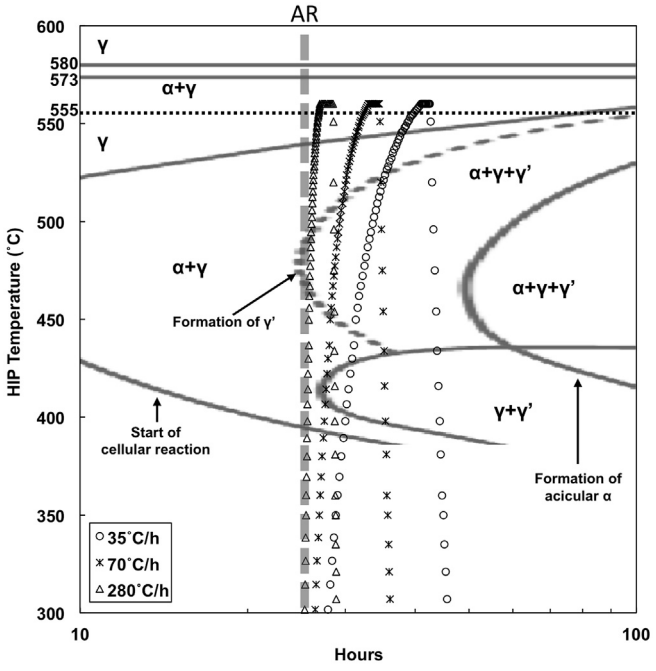

Fig. 9. Thermal history, superimposed on time-temperature-transformation diagram, of the U - 10 wt.% Mo alloy, HIP'ed into monolithic fuel plates at 560 °C for 90 min with a variation in heating/cooling rates of 35, 70 and 280 °C/hour.

Fig. 6 shows microstructure of U10Mo fuel alloy HIP'ed at 560 °C for 90 min with a H/C rate variation of 280, 70 and 35 °C/hour. The micrograph in Fig. 6(a) from the U10Mo alloy with the higher H/C rate of 280 °C/h shows cellular regions along grain boundaries of U10Mo alloy. Cellular structure is better defined than the AR sample, and some of the cellular reaction was observed within the grains of the U10Mo solid solution. For U10Mo alloy HIP'ed with H/C rate of 70 °C/h, a clear development of lamellar structure was observed in addition to the cellular structure as shown in Fig. 6(b). The lamellar structure is assumed to begin from the cellular precipitates along the grain boundaries, and grow into the grain of γ-

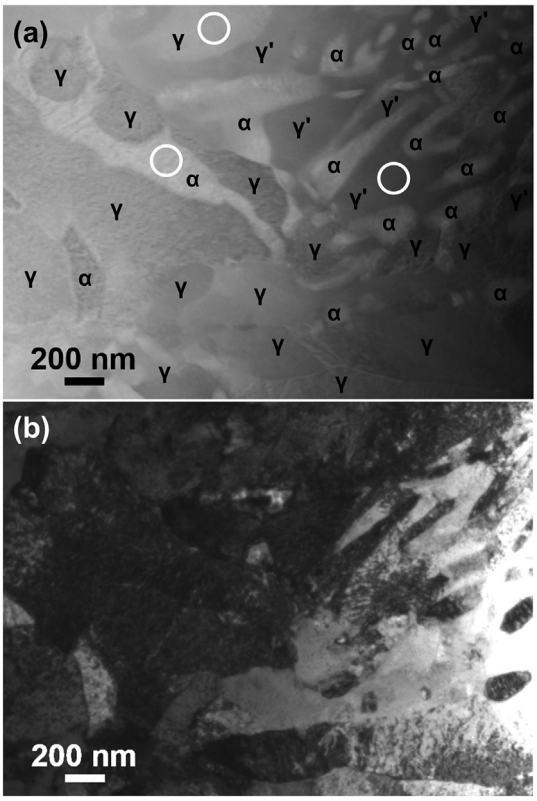

Fig. 10. (a) High angle annular dark field and (b) bright field TEM micrographs from the lamellar region in Fig. 6(c) detailing the decomposition of the γ-U10Mo into α-U and γ′-U_2Mo.

(U10Mo). The largest volume fraction of lamellar structure region was observed in the sample with 35 °C/h H/C rate. The lamellar structure of α and γ′ is presented in detail with a higher magnification BSE micrograph in Fig. 7. Fig. 8 shows that the volume fraction estimated for the lamellar structure region resulting from decomposition of γ increases as the H/C rate decrease. This observation corresponds to the fact that slow H/C rate exposes the U10Mo alloy in the three-phase (α+γ+γ′) region the longest as illustrated on the T-T-T diagram in Fig. 9.

A selected region highlighted by black rectangle in Fig. 6 (c) was prepared by FIB-INLO for TEM analyses presented in Figs. 10 and 11. The SAED patterns presented in Fig. 11 were collected from circled regions in Fig. 10(a). The HAADF and bright-field images shown in Fig. 10 along with SAED patterns presented in Fig. 11 were employed to identify the decomposition of bcc-γ into alternating orthorhombic-α and tetragonal-γ′ lamellar structure. These phases were identified by analyzing the SAED patterns, and the crystallographic characteristics of each phase corresponded well to those reported in Table 2. Variation in Mo composition in g-phase with ~10 wt% Mo, Mo-depleted α, Mo-enriched γ′ was also confirmed by extensive analyses by XEDS equipped on TEM. Other regions consisted of γ and α, without γ'. Therefore the presence of transition region from α+γ to α+γ+γ′ in the T-T-T diagram appears to be consistent with the current TEM analyses.

Fig. 12 shows microstructural variation in U10Mo fuel alloy as a function of HIP temperature. The time at HIP temperature and H/C rate remained constant for 90 min and 280 °C/hour, respectively, for these samples. In general, the volume fractions of cellular and lamellar structure regions decreased with an increase in HIP temperature as presented in Fig. 13. The HIP temperature variation examined in this study is close to the transition that separates γ and

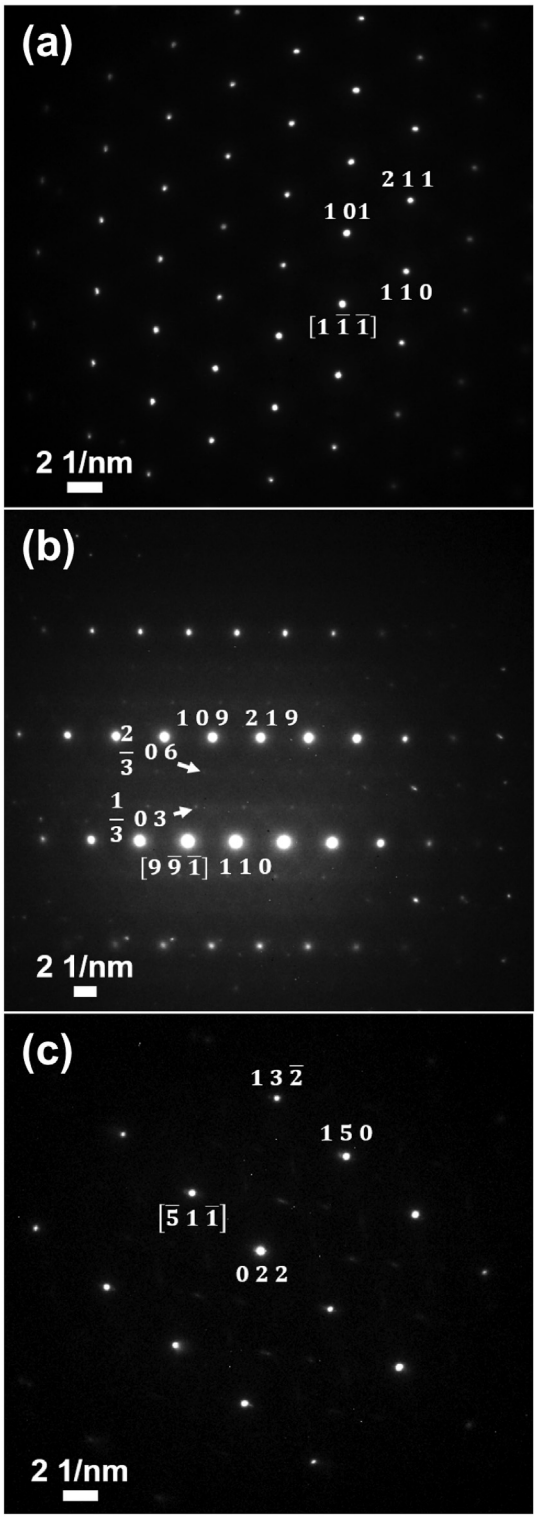

Fig. 11. Selected area electron diffraction patterns from (a) γ-(U10Mo), (b) γ-U_2Mo and (c) α-U collected from circled area shown in Fig. 10(a).

α+γ (and α+γ and γ) on the upper-left-corner of the T-T-T diagram as presented in Fig. 14. Repas *et* al. [26] postulated a transition between α + γ′ and α + γ at 573 °C (lower critical temperature), and between α + γ′ and γ at 580 °C (upper critical temperature) in the T-T-T diagram. However, these temperatures have been subject to some scrutiny by other investigations [14,29,37,38,40,41]. Table 4

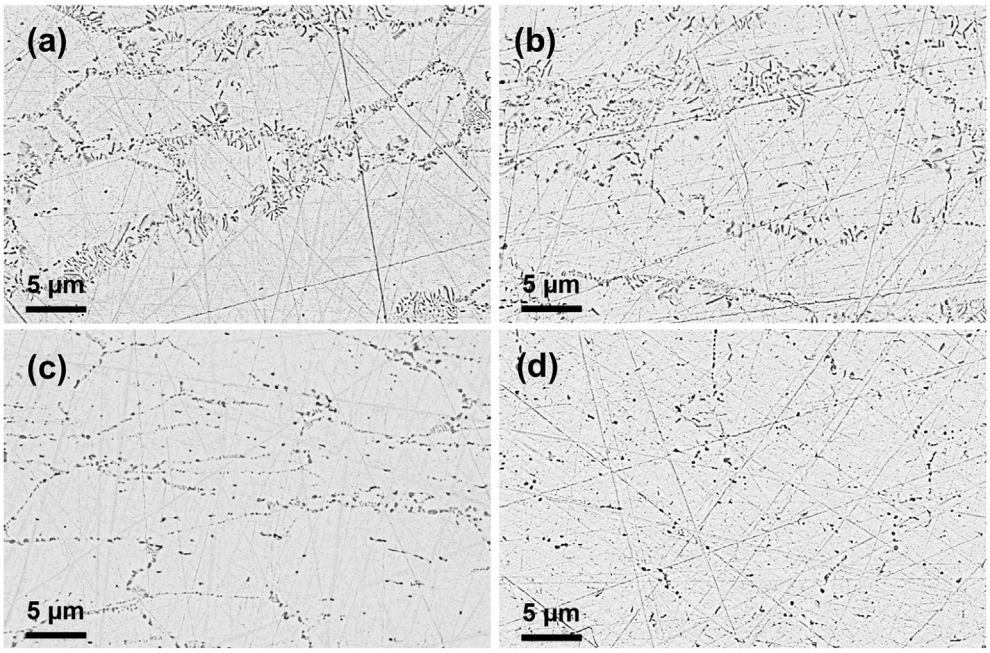

Fig. 12. Backscattered electron micrographs from the U - 10 wt.% Mo alloy, HIP'ed into monolithic fuel plates at (a) 520, (b) 540, (c) 560 and (d) 580 °C. All samples were HIP'ed for 90 min with the same heating/cooling rate of 280 °C/hour.

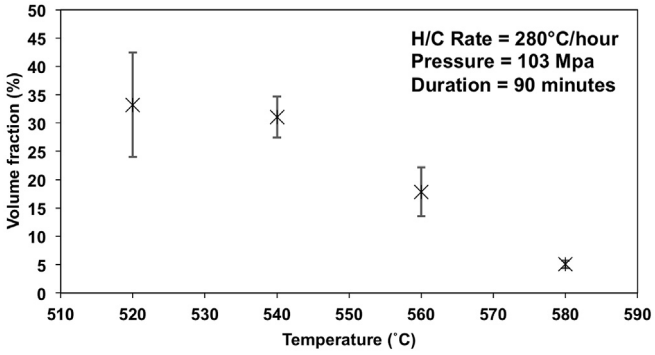

Fig. 13. Volume fraction estimated for the decomposed (i.e., cellular and lamellar structures) region in the U - 10 wt.% Mo alloy, HIP'ed into monolithic fuel plates at (a) 520, (b) 540, (c) 560 and (d) 580 °C. All samples were HIP'ed for 90 min with the same heating/cooling rate of 280 °C/hour.

summarizes the critical transition temperatures reported in literature [14,26,39] for the U − 10 wt% Mo alloy. In this study, the samples HIP'ed at 520 and 540 °C show the lamellar structure of α and γ′ within the γ matrix, while only cellular structure was observed when the samples were HIP'ed at 560 °C and above. This demonstrates the transition of α and γ′ into α and γ starts above 540 °C and below 560 °C.

Effects of HIP holding time was examined with U10Mo alloys HIP'ed at 560 °C with H/C rate of 280 °C/h as presented in Fig. 15. There was no significant change in the amount of decomposed region because, upon heating, a transformation from α+γ' (or α+γ+γ′) into α+γ in the temperature range of 555–580 °C is expected as shown in Fig. 16. Given the HIP temperature of 560 °C, the volume fraction of decomposed region showed no significant trend with HIP holding time, up to 345 min, as shown in Fig. 17. However such an observation may change when HIP temperature is selected at 540 °C or below (e.g., 555 °C according to Okamoto) according to the T-T-T diagram. Therefore, in order to minimize the decomposition of the γ-phase into α- and γ'-phases in the U10Mo fuel, HIP

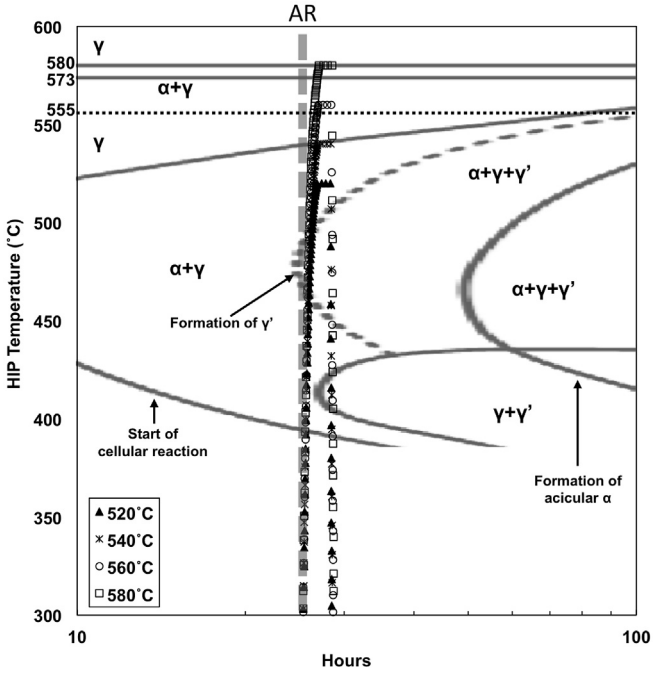

Fig. 14. Thermal history, superimposed on time-temperature-transformation diagram, for the U - 10 wt.% Mo alloy, HIP'ed into monolithic fuel plates at 520°, 540°, 560° and 580 °C for 90 min with a constant heating/cooling rate of 280 °C/hour.

Table 4
The critical temperature reported in literature [14,26,39] for $\alpha + \gamma' \rightarrow \alpha + \gamma$ and $\alpha + \gamma \rightarrow \gamma$ transitions in the U − 10 wt% Mo alloy.

	$\alpha + \gamma' \rightarrow \alpha + \gamma$ (lower critical temperature)	$\alpha + \gamma \rightarrow \gamma$ (upper critical temperature)
Repas [26]	573 °C	580 °C
Kim [39]	N/R	>570
Okamoto [13]	555 °C	~580 °C

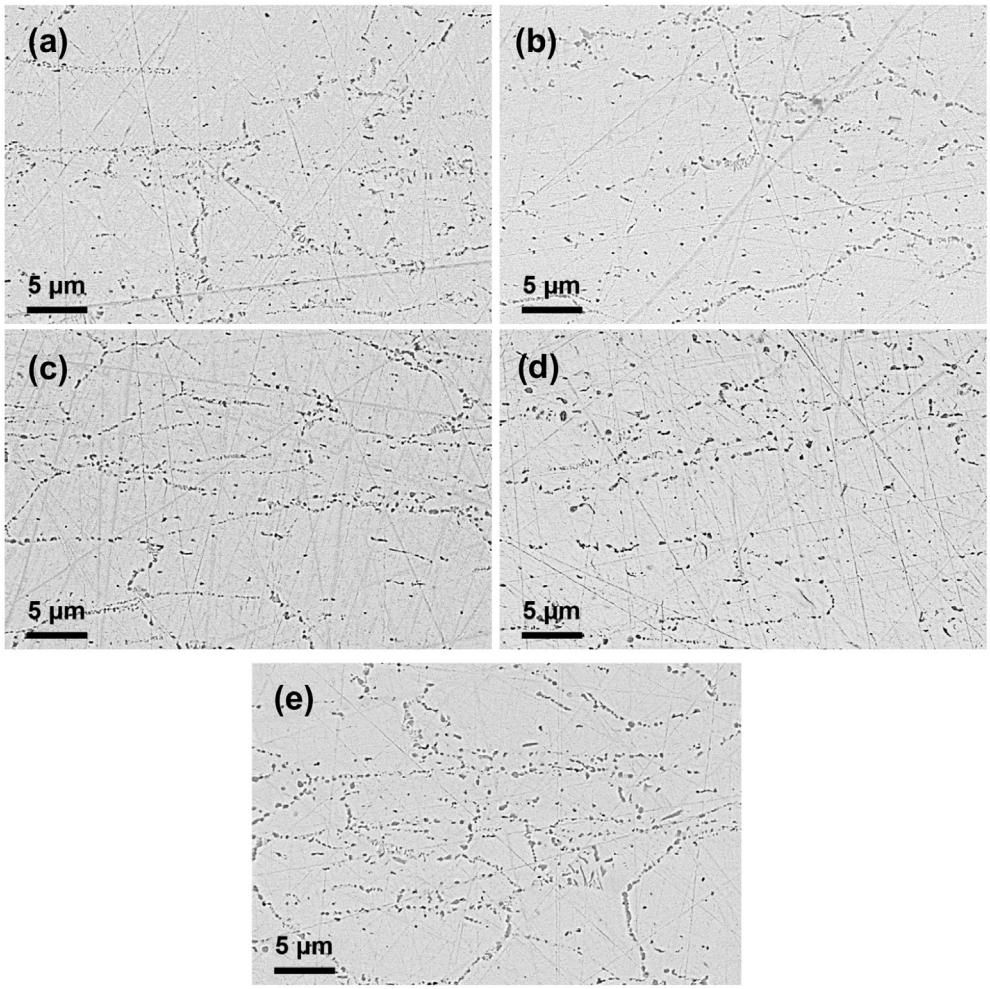

Fig. 15. Backscattered electron micrographs for the U - 10 wt.% Mo alloy, HIP'ed into monolithic fuel plates at 560 °C for (a) 45, (b) 60, (c) 90, (d) 180 and (e) 345 min with a constant heating/cooling rate of 280 °C/hour.

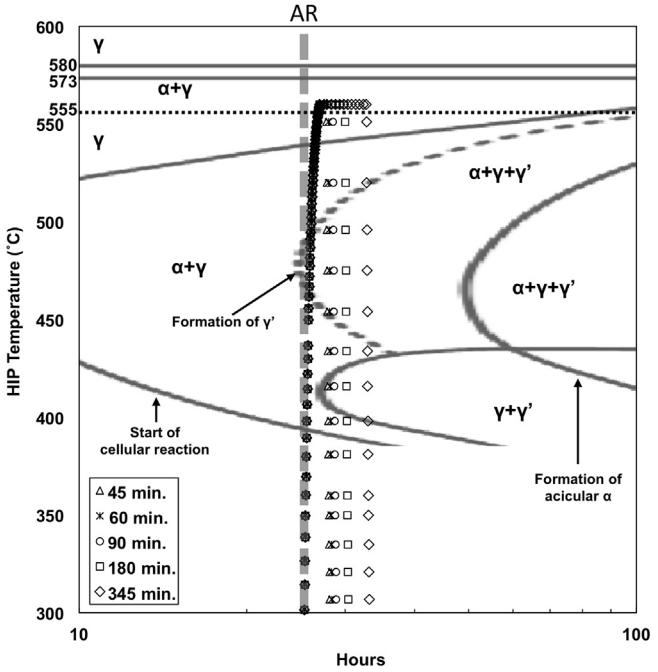

Fig. 16. Thermal history, superimposed on time-temperature-transformation diagram, for the U - 10 wt.% Mo alloy, HIP'ed into monolithic fuel plates at 560 °C for 45, 60, 90, 180 and 345 min with a constant heating/cooling rate of 280 °C/hour.

utilizing at least 560 °C and the highest H/C rate would be recommended. HIP at 580 °C may allow longer duration without concern for any decomposition.

A related consideration for higher HIP temperature is the interdiffusion and reaction among U10Mo fuel alloy, Zr diffusion barrier, and AA6061 cladding alloy. In our previous study, HIP did not cause any observable growth of the interaction layer at the U10Mo/Zr interface within the temperatures and holding time

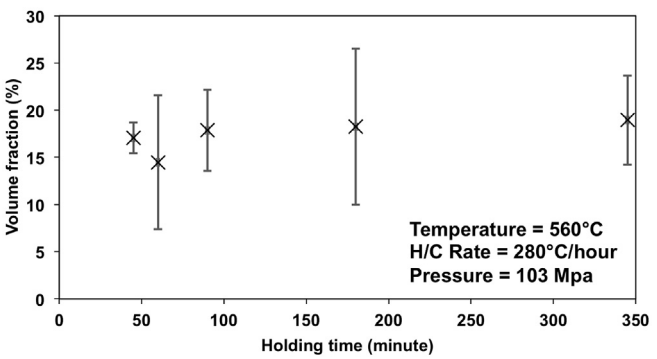

Fig. 17. Volume fraction estimated for the decomposed (i.e., cellular and lamellar structures) region in the U - 10 wt.% Mo alloy, HIP'ed into monolithic fuel plates at 560 °C for 45, 60, 90, 180 and 345 min with a constant heating/cooling rate of 280 °C/hour.

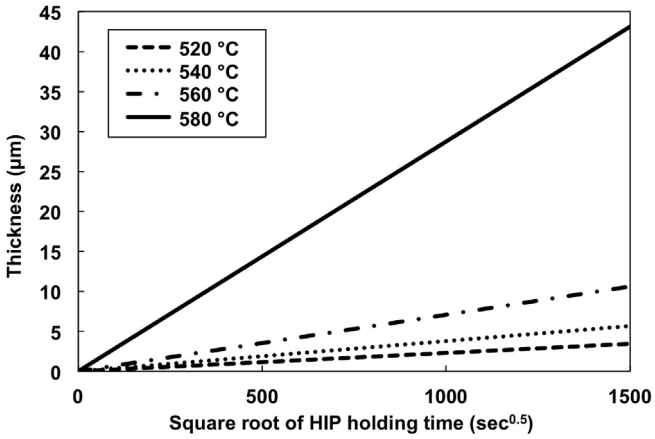

Fig. 18. Estimated thickness of $(Al,Si)_3Zr$ as a function of HIP temperature and duration [9].

range examined [9]. Development of the interaction layer containing α-U, UZr_2, and Mo_2Zr at the U10Mo/Zr interface primarily occurred during the co-rolling process (650 °C) prior to HIP. However, the intermetallic $(Al,Si)_3Zr$ at the AA6061/Zr interface was observed to grow with the HIP duration, and the growth followed the Arrhenius relation with an activation energy of 457.54 ± 27.60 kJ/mol. Fig. 18 illustrates the growth kinetics of $(Al,Si)_3Zr$ at the AA6061/Zr interface [9]. Therefore the HIP process for the monolithic fuel system should employ higher temperature (e.g., 560° and 580 °C) to (1) ensure the highest quality of adhesion at the U10Mo/Zr and AA6061/Zr interfaces [9,10], and (2) minimize the γ-phase decomposition, (3) however, without excessive growth of $(Al,Si)_3Zr$ layer at the AA6061/Zr.

5. Conclusion

U − 10 wt% Mo alloy for the monolithic fuel plates encased in AA6061 cladding with Zr barrier was characterized as functions of HIP parameters with an emphasis on decomposition of γ-phase into α- and γ'-phases. From TEM SAED, the constituent phases of the U10Mo alloy consisted of γ cI2 Im3m (3.474 × 3.474 × 3.474 Å), α oC4 Cmcm (2.854 × 5.869 × 4.955 Å) and γ′ tI6 I4/mmm (3.427 × 3.427 × 9.834 Å). The α- and γ'-phases formed by decomposition of the γ-phase because the HIP process was carried out near the eutectoid temperature with varying HIP parameters including ramping/cooling rate, temperature, and holding time. Initially, a cellular structure of α and γ′ from the decomposition of γ developed discontinuously on grain boundaries, and evolved into lamellar structures of alternating α and γ'. Volume fraction associated with decomposition (e.g., cellular and lamellar structure) decreased with (1) an increase in ramping/cooling rate, (2) an increase in HIP temperature due to γ-phase stabilization at higher temperature. There was no significant development of decomposed lamellar structure when the HIP was carried out at 560 °C for up to 345 min.

Acknowledgements

The work was supported by the US Department of Energy under DOE-NE Idaho Operations Office Contract DE-AC07-05ID14517 administered by Battelle Energy Alliance, LLC. The U. S. Government retains and the publisher, by accepting the article for publication, acknowledges that the U. S. Government retains a nonexclusive, paid-up, irrevocable, world-wide license to publish or reproduce the published form of this manuscript, or allow others to do so, for U.S. Government purposes. U. S. Department of Energy DisclaimerThis information was prepared as an account of work sponsored by an agency of the U. S. Government. Neither the U. S. Government nor any agency thereof, nor any of their employees, makes any warranty, express or implied, or assumes any legal liability or responsibility for the accuracy, completeness, or usefulness of any information, apparatus, product, or process disclosed, or represents that its use would not infringe privately owned rights. References herein to any specific commercial product, process, or service by trade name, trademark, manufacturer, or otherwise, does not necessarily constitute or imply its endorsement, recommendation, or favoring by the U. S. Government or any agency thereof. The views and opinions of authors expressed herein do not necessarily state or reflect those of the U. S. Government or any agency thereof.

References

[1] A. Travelli, "The effect of reduced enrichment on the fuel cycle for Research reactors," The International Topical Meeting on Nuclear Fuel Cycles and Waste Disposal, Brussels, Belgium, 1982, IAEA-CONF-820420–12.
[2] J.L. Snelgrove, G.L. Hofman, M.K. Meyer, C.L. Trybus, T.C. Wiencek, Nucl. Eng. Des. 178 (1997) 119–126.
[3] D.D. Keiser Jr., S.L. Hayes, M.K. Meyer, C.R. Clark, J. Met. 55 (2003) 55–58.
[4] S. Van Den Berghe, A. Leenaers, E. Koonen, L. Sannen, Adv. Sci. Technol. 73 (2010) 78–90.
[5] A.B. Robinson, G.S. Chang, D.D. Keiser Jr., D.M. Wachs, D.L. Porter, Irradiation Performance of U-Mo Alloy Based "Monolithic" Plate-type Fuel – Design and Selection, Idaho National Laboratory, Idaho Falls, Idaho, 2009. INL/EXT-09–16807.
[6] Y.S. Kim, Uranium intermetallic fuels (U-Al, U-Si, U-Mo), in: R.J.M. Konings (Ed.), Comprehensive Nuclear Materials, vol. 3, Elsevier, 2012, pp. 391–422.
[7] G.L. Hofman, M.K. Meyer, Progress in irradiation performance of experimental uranium-molybdenum dispersion fuel, in: The 24th Interational Meeting on Reduced Enrichment for Research and Test Reactors, San Carlos de Bariloche, Argentina, 2002.
[8] Y. Park, N. Eriksson, D.D. Keiser Jr., J.F. Jue, B. Rabin, G. Moore, Y.H. Sohn, Mater. Charact. 103 (2015) 50–57.
[9] Y. Park, J. Yoo, K. Huang, D.D. Keiser Jr., J.F. Jue, B. Rabin, G. Moore, Y.H. Sohn, J. Nucl. Mater. 447 (2014) 215–224.
[10] E. Perez, B. Yao, D.D. Keiser Jr., Y.H. Sohn, J. Nucl. Mater. 402 (2010) 8–14.
[11] M.K. Meyer, G.A. Moore, J.F. Jue, D.D. Keiser Jr., I.Y. Glagolenko, D.M. Wachs, P.E. Murray, A.B. Robinson, F.J. Rice, H. Ozaltun, S.J. Miller, M.A. Okuniewski, B.H. Rabin, H.W. Glunz, N.J. Lybeck, Investigation of the Cause of Low Blister Threshold Temperatures in the RERTR-12 and AFIP-4 Experiments, Idaho National Laboratory, 2012. INL/EXT-12–26500.
[12] J.-F. Jue, D.D. Keiser Jr., C.R. Breckenridge, G.A. Moore, M.K. Meyer, J. Nucl. Mater. 448 (2014) 250–258.
[13] G.A. Moore, F.J. Rice, N.E. Woolstenhulme, W.D. Swank, D. Haggard, J. Jue, B.H. Park, S.E. Steffler, N.P. Hallinan, M.D. Chapple, D.E. Burkes, Monolithic fuel fabrication process development at the Idaho national laboratory, in: The 30th International Meeting on Reduced Enrichment for Research and Test Reactors, Washington, DC, USA, 2008.
[14] H. Okamoto, J. Phase Equilibria Diffus. 33 (2012) 497.
[15] H.L. Yakel, A review of x-ray diffraction studies in uranium alloys, in: The Physical Metallurgy of Uranium Alloys Conference, 1974. ORNL-CONF-740205–9.
[16] C.V. Sundaram, S.L. Mannan, Sadhana 14 (1989) 21–57.
[17] M. Lehmann, J. Nucl. Mater. 2 (1960) 261–268.
[18] R.L. Miller, G.A. Reimann, Thermodynamics of Gas-metal-slag Equilibria for Applications in in Situ and Ex Situ Vitrification Melts, Idaho National Engineering Laboratory, 1993. EGG-MS-10613.
[19] M.M. Baker, L.N. Less, S. Orman, Trans. Faraday Soc. 62 (1966) 2525–2530.
[20] J.M. Macki, R.L. Kochen, Corrosion Behavior of Uranium-Base U-NB, U-NB-Zr, and U-Mo Alloys in Hydrochloric Acid and Ocean Water, US Atomic Energy Commission, 1971, http://dx.doi.org/10.2172/4051383.
[21] V.F. Peretrukhin, A.G. Maslennikov, A.Y. Tsivadze, C.H. Delegard, A.B. Yusov, V.P. Shilov, A.A. Bessonov, K.E. German, A.M. Fedoseev, L.P. Kazanskii, N.Y. Budanova, A.V. Kareta, A.V. Gogolev, K.N. Gedgovd, G.S. Bulatov, Prot. Met. 44 (2008) 211–232.
[22] W.R. McDonell, G.R. Caskey, C.L. Angerman, High-performance Uranium-metal Fuels for Savannah River Reactors, Westinghouse Savannah River Company, 1975. WSRC-MS-2000–00061.
[23] G. Beghi, Gamma Phase Uranium-molybdenum Fuel Alloys, European Atomic Energy Community - Euratom, 1968. EUR 4053e.
[24] M.K. Meyer, J. Gan, J.F. Jue, D.D. Keiser Jr., E. Perez, A. Robinson, D.M. Wachs, N. Woolstenhulme, G.L. Hofman, Y.S. Kim, Nucl. Eng. Technol. 46 (2014) 169–182.

[25] International Atomic Energy Agency, Development Status of Metallic, Dispersion and Non-oxide Advanced and Alternative Fuels for Power and Research Reactors, 2003. Vienna, IAEA-TECDOC-1374.
[26] P.E. Repas, R.H. Goodenow, R.F. Hehemann, Trans. ASM 57 (1964) 150–163.
[27] C.A.W. Peterson, W.J. Steele, S.L. DiGiallonardo, Isothermal Transformation Study of Some Uranium-base Alloys, University of California Lawrence Radiation Laboratory, 1964.
[28] S. Neogy, M.T. Saify, S.K. Jha, D. Srivastava, M.M. Hussain, G.K. Dey, R.P. Singh, J. Nucl. Mater. 422 (2012) 77–85.
[29] G.L. Hofman, M.K. Meyer, A.E. Ray, in: The 21th International Meeting on Reduced Enrichment for Research and Test Reactors, Sao Paulo, Brazil, 1998.
[30] B.-S. Seong, C.-H. Lee, J.-S. Lee, H.-S. Shim, J.-H. Lee, K.H. Kim, C.K. Kim, V. Em, J. Nucl. Mater. 277 (2000) 274–279.
[31] K. Huang, C.C. Kammerer, D.D. Keiser Jr., Y.H. Sohn, J. Phase Equilibria Diffus. 35 (2014) 146–156.
[32] S. Jaroszewicz, E.L. Losada, J.E. Garcés, H.O. Mosca, J. Nucl. Mater. 441 (2013) 119–124.
[33] V.P. Sinha, P.V. Hegde, G.J. Prasad, G.K. Dey, H.S. Kamath, J. Alloys. Compd. 506 (2010) 253–262.
[34] N.-T.H. Kim-Ngan, I. Tkach, S. Mašková, L. Havela, A. Warren, T. Scott, Adv. Nat. Sci. Nanosci. Nanotechnol. 4 (2013) 035006.
[35] V.P. Sinha, P.V. Hegde, G.J. Prasad, G.K. Dey, H.S. Kamath, J. Alloys. Compd. 491 (2010) 753–760.
[36] H.A. Saller, F.A. Rough, A.A. Bauer, Transformation kinetics of uranium-molybdenum alloys, U.S. Atomic Energy Commission, Battelle Memorial Institute, 1955. BMI 957.
[37] R.M. Willard, A.R. Schmitt, Irradiation Swelling, Phase Reversion, and Intergranular Cracking of U-10wt.%Mo Fuel Alloy, Atomics International, 1965. NAA-SR-8956.
[38] K.H. Kim, H.J. Kwon, J.M. Park, Y.S. Lee, C.K. Kim, J. Korean Nucl. Soc. 33 (2001) 365–374.
[39] A.L. Lotts, Review of Information on U-Mo Alloys and U-Mo-UO2 Dispersion Fuels, Oak Ridge National laboratory, 1960. ORNL-60-6-122.
[40] P.E. Armstrong, D.T. Eash, J.E. Hockett, J. Nucl. Mater. 45 (1972) 211–216.
[41] S.D. Cramer, B.S. Covino Jr., ASM Handbook Volume 13, Corrosion: Materials, ASM International, 2003.
[42] V.F. Sears, Neutron News 3 (1992) 26–37.
[43] W. Martienssen, H. Warlimont, Springer Handbook of Condensed Matter and Materials Data, Springer Berlin Heidelberg, 2006.
[44] E.K. Halteman, Acta Crystallogr. 10 (1957) 166–169.
[45] F.A. Rough, A.A. Bauer, Constitution of Uranium and Thorium Alloys, Battelle Memorial Institute, 1958. BMI-1300.
[46] A.E. Dwight, J. Nucl. Mater. 2 (1960) 81–87.
[47] R.J. Jackson, Structure and Transformation Kinetics of Phases in the Uranium-rhenium Alloy System, Ph.D. Dissertation in Metallurgy, Iowa State University, Ames, Iowa, 1964, p. 162.
[48] S.L. Robinson, J. Nucl. Mater. 46 (1973) 293–302.
[49] D.E. Burkes, G.S. Mickum, D.M. Wachs, Thermophysical Properties of U-10Mo Alloy, Idaho National Laboratory, 2010. INL/EXT-10–19373.
[50] D.E. Burkes, R. Prabhakaran, T. Hartmann, J.-F. Jue, F.J. Rice, Nucl. Eng. Des. 240 (2010) 1332–1339.
[51] T.R.G. Kutty, S. Dash, J. Banerjee, S. Kaity, A. Kumar, C.B. Basak, J. Nucl. Mater. 420 (2012) 193–197.